MINIMUM SYMBOL ERROR RATE TIMING RECOVERY SYSTEM

by

Nagendra Bage Jayaraj

A thesis submitted in partial fulfillment
of the requirements for the degree

of

MASTER OF SCIENCE

in

Electrical Engineering

Approved:

Dr. Jacob Gunther Major Professor	Dr. Todd Moon Committee Member
Dr. Edmund Spencer Committee Member	Dr. Byron R. Burnham Dean of Graduate Studies

UTAH STATE UNIVERSITY
Logan, Utah

2010

Abstract

Minimum Symbol Error Rate Timing Recovery System

by

Nagendra Bage Jayaraj, Master of Science

Utah State University, 2010

Major Professor: Dr. Jacob Gunther
Department: Electrical and Computer Engineering

This thesis presents a timing error detector (TED) used in the symbol timing synchronization subsystem for digital communications. The new timing error detector is designed to minimize the probability of symbol decision error, and it is called minimum symbol error rate TED (MSERTED). The new TED resembles the TED derived using the maximum likelihood (ML) criterion but gives rise to faster convergence relative to MLTED. The new TED requires shorter training sequences for symbol timing recovery. The TED operates on the outputs of the matched filter and estimates the timing offset. The S-curve is used as a tool for analyzing the behavior of the TEDs. The faster convergence of the new TED is shown in simulation results as compared to MLTED. The new TED works well for any two-dimensional constellation with arbitrarily shaped decision regions.

(44 pages)

To my beloved family, friends, and my soul Parinita.

Acknowledgments

This research project would have never been completed without my advisor and mentor, Dr. Jacob Gunther. This project is the outcome of his constant motivation and belief in me. I would have never been able to complete this research without his guidance, patience, and expertise in the field of digital signal processing (DSP) and communications. His courses provided the foundation for my research and helped me become a better researcher. I am grateful, and thank him for all his guidance, support, and valuable time. I would also like to thank my committee members, Dr. Todd Moon and Dr. Edmund Spencer, for extending their support.

Also, I would like to thank my father, P Jayaraj, who has been always supporting me in whatever I do; and my mother, Uma Jayaraj, who has been the inspiration in my life. I would like to thank my sister, Bhavya, and brother-in-law, Hrishikesh, who have always given me the moral support at critical times. I would like to thank my niece, Parinita, who is very special to me. She is the one who brings a smile to my face. I would like to thank Dr. David Hailey and Dr. Chris Hailey for their support during my stay at USU. Finally, I would like to acknowledge my friends, especially Reddy, Loki, Shantha, Balu, Koli, Barey, Dharnish, Kiran, Atul, Karthik, Amrita, Chandu, Kalyan, Pradeep, Hema Swaroop, Rahul, and Nagaravind, with whom I have spent the best times of my student life.

Nagendra Bage Jayaraj

Contents

List of Figures

Chapter 1

Introduction

In digital communication, the transmitter uses a clock to generate the waveform transmitted over the channel. The receiver synchronization problem is to find the correct sampling instances to recover the transmitted data symbols at the matched filter output. In order to efficiently use the available spectrum, the clock used for data generation at the transmitter cannot be transmitted separately to the receiver for the purpose of timing synchronization. If a separate clock is transmitted from transmitter, then the transmitter has to allocate some of its available power for the transmission of clock, which is not desirable. As the number of users increase, transmitting a separate clock becomes practically impossible. Hence, most of the time the clock signal in the receiver must be recovered from the noisy received data and will be used for receiver operations. In the case of matched filter detectors, the outputs of the matched filter are sampled using the synchronized clock at the receiver. Ideally, it is desirable to sample the matched filter outputs at the center of the eye diagram. The timing offset in the clock will lead to offsets in the sampling instances of the eye diagram. Hence in a synchronous digital communication system, symbol timing recovery at the receiver plays a critical role. The receiver should know the sampling instant in the symbol period with duration T_s and frequency $\frac{1}{T_s}$ at which matched filter outputs need to be sampled. As shown in the eye patterns in figs. 1.1 and 1.2 for quadrature phase shift keying (QPSK), when the matched filter outputs are sampled with a timing offset, the received signal space projections are scattered. The scattering of signal space projection in the absence of noise is illustrated in figs. 1.1 and 1.2 and the situation becomes worse in the presence of noise. The pulse shape used is a square root raised cosine (SRRC) pulse with 50% excess bandwidth.

The timing recovery system consists of a phase locked loop (PLL) which contains three

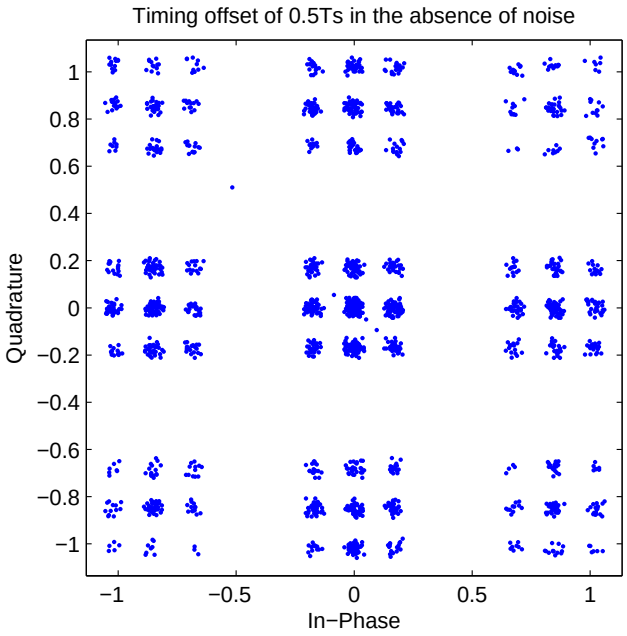

Fig. 1.1: Scatter plot with timing offset of $0.5T_s$ in the absence of noise.

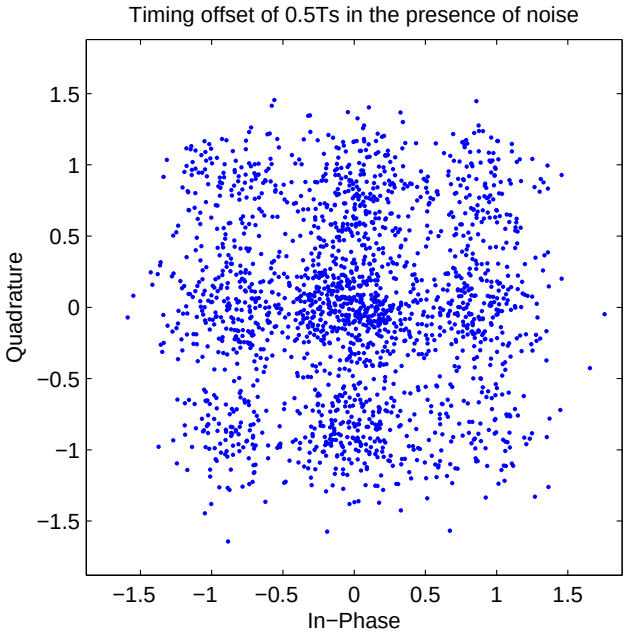

Fig. 1.2: Scatter plot with timing offset of $0.5T_s$ in the presence of noise.

components: a timing error detector (TED), a loop filter and an interpolator controlled by an interpolation control block. The timing error detector outputs the error signal e which is related to the difference between the unknown timing offset τ and the estimate of the timing offset $\hat{\tau}$. The PLL adjusts the estimate $\hat{\tau}$ to be close to the timing offset τ and forces the error signal to be zero.

A widely used optimization criterion in deriving the timing and phase recovery systems is the maximum likelihood (ML) criterion [1, 2]. The problem of carrier phase and symbol timing recovery for baseband pulse amplitude modulation (PAM) was examined by Franks [3]. Meyers and Franks [4] explored the problem of symbol timing and carrier phase estimation for PAM using both data-aided (DA) estimators and nondata-aided (NDA) estimators. The log-likelihood ratio L is differentiated with respect to τ_e to obtain the error signal and the equation $\frac{dL}{d\tau_e} = 0$ is solved by the PLL. In case of MSER, the logarithm of probability of error is used as the criterion to obtain the error signal used for the synchronization.

The probability of error criterion is widely used as an alternative to the traditional mean-squared approaches for addressing the digital communications problems. Gunther and Moon [5] use this approach to derive the minimum symbol error rate phase recovery system. Aaron and Tufts [6] showed that the average minimum probability of error receiver for binary PAM transmitted through a noisy and dispersive medium consists of a linear filter which is the matched filter itself followed by a tapped delay line. Yen [7] and Chen et al. [8] derive decision feedback equalizers using the minimum error rate probability condition along with the use of stochastic gradient approach. It is also pointed out that, in general, MSER algorithms work well and are never trapped at locally minimizing solutions. Gunther and Moon [9] use Bayes risk in deriving the minimum Bayes risk adaptive linear equalizers which can be applied to any two-dimensional constellations with arbitrarily shaped decision regions. Yeh and Barry [10, 11] use error probability to derive adaptive linear equalizers. Yeh et al. [12], Chen et al. [13], Wang et al. [14], and Psaromiligkos et al. [15] investigate minimum bit error rate multi-user detection. Minimum bit error rate beamformers in a

multi-antenna communication scenario were developed by Chen et al. [16] and Samir et al. [17]. Most of the prior work centers on the M-ary quadrature amplitude modulation (QAM) where the decision boundaries are rectangular. But in case of MSERTED, the two-dimensional constellations can have arbitrarily shaped decision regions.

The maximum likelihood timing error detector (MLTED) uses the slope of the eye diagram to produce the error signal. There exist two flavors of MLTED, namely the data-aided case and the nondata-aided case. A more general class of data aided MLTED was developed by Bergmans and Wong [18]. The early-late timing error detector (ELTED) approximates the derivative required by MLTED using time differences. The zero-crossing timing error detector (ZCTED) works on the zero crossings of the eye diagram. It operates at two samples/symbol on the matched filter outputs. The Gardner timing error detector (GTED) was developed by Gardner [19]. The algorithm was intended for synchronous binary phase shift keying (BPSK) and QPSK. The GTED is not decision directed and the clock recovery is independent of carrier phase recovery. Mueller an Muller [20] developed a TED called Mueller-Muller TED (MMTED) which operates at one sample/symbol period and convergence is exponential. One of the important performance evaluation parameters of these TEDs is the self noise. MLTED and ELTED have more self noise when compared to ZCTED, GTED, and MMTED. The MSERTED has higher self noise than MLTED.

This thesis is organized in the following manner. Chapter 2 presents the data model and probability of error modeling along with the S-curves which are used as a tool for the analysis of the new TED. Chapter 3 discusses the implementation of the timing recovery system. Chapter 4 discusses the performance of MSERTED against MLTED using simulation results. Finally, Chapter 5 concludes the thesis and suggests some future work.

Chapter 2

Datamodel

2.1 Datamodel

This chapter describes the datamodel and the probability of error modeling used to derive the MSERTED. The S-curves are derived to gain an insight on the behavior of the MSERTED as compared to MLTED.

Let $\mathcal{A} = \{c_1, c_2, \cdots, c_M\}, M = 2^b$, define a constellation of complex symbols, (i.e., $c_i \in \mathbb{C}$ for all i). A transmitter randomly selects symbols $a(n) \in \mathcal{A}$ and transmits them over an intersymbol interference (ISI) channel at a rate of $1/T_s$ symbols per second.

The received signal at the matched filter input is:

$$r(t) = G \sum_n a(n)\, p(t - nT_s - \tau) + u(t), \tag{2.1}$$

where $a(n) \in$ constellation $\mathcal{A}$, G is the composite of all the amplitude gains and losses occurred during transmission, $p(t)$ is the square root raised cosine (SRRC) pulse with unit energy and support in the interval $-L_pT_s \leq t \leq L_pT_s$, τ is the unknown timing delay, $u(t)$ is white Gaussian noise with variance σ^2.

The received signal is passed through the matched filter with impulse response $p(-t)$. The output of the matched filter (MF) is given by:

$$x(t) = G \sum_n a(n)\, r_p(t - nT_s - \tau) + v(t), \tag{2.2}$$

where $r_p(t)$ is the autocorrelation function of the pulse shape given by eq. (2.3). The term $v(t)$ represents the noise at the MF output given by eq. (2.4) and $*$ in eq. (2.4) represents

the convolution operation.

$$r_p(t) = \int_{L_pT_s}^{-L_pT_s} p(u)\, p(u-t)\, du \tag{2.3}$$

$$v(t) = u(t) * p(-t) \tag{2.4}$$

Let the matched filter output be sampled at N samples per symbol period, (i.e., $T = T_s/N$). Ideally, the matched filter output should be sampled at $t = kT_s + \tau$. Let $\hat{\tau}$ be the estimate of τ. Therefore, the sampled version of matched filter output is given by:

$$x(kT + \hat{\tau}) = G_a \sum_n a(n)\, r_p(kT + \hat{\tau} - nT_s - \tau) + v(kT + \hat{\tau}). \tag{2.5}$$

Substituting $k = nN$ for downsampling to the symbol rate and rearranging (2.5) we get:

$$x(nT_s + \hat{\tau}) = G \sum_i a(i)\, r_p((n-i)T_s - \tau_e) + v(nT_s + \hat{\tau}), \tag{2.6}$$

where $\tau_e = \tau - \hat{\tau}$ is the timing error which is the difference between actual timing delay and the estimated one.

The vector form of (2.6) can be written as:

$$y_n = x(nT_s + \hat{\tau}) = \mathbf{r}_p^T(\tau_e)\, \mathbf{s}_n + v_n, \tag{2.7}$$

where

$$\mathbf{r}_p^T(\tau_e) = [r_p(-L_pT_s - \tau_e), \cdots, r_p(-\tau_e), \cdots, r_p(L_pT_s - \tau_e)],$$

and

$$\mathbf{s}_n = [a(n + L_p), \cdots, a(n), \cdots, a(n - L_p)]^T.$$

Also define $\mathbf{s}_n[c_i]$, a symbol vector of dimensions $(2L_p+1)\times 1$ as follows:

$$\mathbf{s}_n[c_i] = \left[a\left(n+L_p\right), \cdots, c_i, \cdots, a\left(n-L_p\right)\right]^T. \tag{2.8}$$

2.2 Probability of Error

In this section, the probability of error is calculated as a function of τ_e which eventually leads to error signal equation and also helps to plot S-curves. Let $\mathbf{s}_n[c_i]$ be equal to the vector $\mathbf{s}_n$ except for the L_p+1^{th} element from the top of the vector, which is equal to c_i. We want the decision output based on y_n to be equal to c_i. The probability of error is given by:

$$\begin{aligned} P\left(e\right) &= \sum_{i=1}^{M} P\left(e|a(n)=c_i\right) P\left(a(n)=c_i\right) \\ &= \frac{1}{M}\sum_{i=1}^{M} P\left(e|a(n)=c_i\right), \end{aligned} \tag{2.9}$$

where uniform prior probability on symbols is assumed. Introducing variables and marginalizing them out we get:

$$\begin{aligned} P\left(e\right) &= \frac{1}{M}\sum_{i=1}^{M}\sum_{\text{other }\mathbf{C}} P\left(e, \left(a\left(n+L_p\right)=\text{other } c, \cdots, a\left(n-L_p\right)=\text{other } c\right)|a(n)=c_i\right) \\ &= \frac{1}{M}\sum_{i=1}^{M}\sum_{\text{other }\mathbf{C}} P\left(e|\mathbf{s}_n\left[c_i\right]=\text{other } \mathbf{c}\right) P_{\text{prior}}\ , \end{aligned} \tag{2.10}$$

where

$$P_{\text{prior}} = P\left(\left(a\left(n+L_p\right)=\text{other } c, \cdots, a\left(n-L_p\right)=\text{other } c\right)|a(n)=c_i\right).$$

Since the symbols are independent, the conditioning can be dropped. Hence, the term $P\left(\left(a\left(n+L_p\right)=\text{other } c, \cdots, a\left(n-L_p\right)=\text{other } c\right)|a(n)=c_i\right)$ in (2.10) represents the prior

probability and is equal to $\frac{1}{M^{2L_p}}$. Therefore (2.10) can be simplified as

$$\begin{aligned} P(e) &= \frac{1}{M}\sum_{i=1}^{M}\frac{1}{M^{2L_p}}\sum_{\text{other}\mathbf{C}} P\left(e|\mathbf{s}_n\left[c_i\right]=\text{other }\mathbf{c}\right) \\ &= \frac{1}{M^{2L_p+1}}\sum_{i=1}^{M}\sum_{\text{other}\mathbf{C}} P\left(e|\mathbf{s}_n\left[c_i\right]=\text{other }\mathbf{c}\right) \qquad (2.11) \\ &= \frac{1}{M}\sum_{i=1}^{M}\sum_{j=1,j\neq i}^{M} E_{\mathbf{s}_n[c_i]} P\left(e|\mathbf{s}_n\left[c_i\right]=c_j\right). \qquad (2.12) \end{aligned}$$

The term $P\left(e|\mathbf{s}_n\left[c_i\right]=c_j\right)$ in eq. (2.12) represents the probability that $\mathbf{s}_n[c_i]$ symbol vector was transmitted and the decision was made as some other symbol c_j of the constellation with $j \neq i$.

The following lemma helps establish a relationship between the term $P\left(e|\mathbf{s}_n\left[c_i\right]=c_j\right)$ and the probability of error involving symbol decision regions shown in fig. 2.1.

Lemma 1 *Given the constellation $\mathcal{A}=\{c_1, c_2, \cdots, c_M\}$, let $\mathcal{R}_i, i=1,2,\cdots,M$, be a disjoint covering of $\mathbb{C}$ in which the individual regions are given by:*

$$\mathcal{R}_i = \{y : |y-c_i| < |y-c_j| \ \textit{ for all } j \neq i\}. \qquad (2.13)$$

Choose two symbols c_i and c_j from $\mathcal{A}$ and define the pair of disjoint regions

$$\begin{aligned} \mathcal{S}_i &= \{y : |y-c_i| < |y-c_j|\}, \\ \mathcal{S}_j &= \{y : |y-c_j| < |y-c_i|\}, \end{aligned} \qquad (2.14)$$

which cover $\mathbb{C}$. Then

$$P(y_n \in \mathcal{R}_j|\mathbf{s}_n[c_i]) \leq P(y_n \in \mathcal{S}_j|\mathbf{s}_n[c_i]). \qquad (2.15)$$

Proof: The proof is based on $\mathcal{R}_j \subset \mathcal{S}_j$ which follows from the definitions of the regions in (2.13) and (2.14) [9].

Note that equality is achieved in (2.15) when $\mathcal{A}$ consists of just two points. Furthermore, equality is approximately achieved when c_i and c_j are neighbors in a large constellation and the signal-to-noise ratio is high.

Figure 2.1 [9] shows two symbols c_i and c_j in the square 16-QAM constellation. This picture illustrates the regions defined in Lemma 1. The dashed lines are the minimum distance decision region boundaries; the region $\mathcal{R}_j$ for the j^{th} symbol c_j is shaded a dark gray. The regions $\mathcal{S}_j$ (shaded light gray) and $\mathcal{S}_i$ (white) are also shown with a dotted line marking the boundary separating these two regions.

Using Lemma 1 the probability of error in (2.12) can be written as:

$$P(e) = \frac{1}{M} \sum_{i=1}^{M} \sum_{j=1, j\neq i}^{M} E_{\mathbf{s}_n[c_i]} P\left(y_n \in S_j | \mathbf{s}_n[c_i]\right). \tag{2.16}$$

The following lemma helps to further simplify the term $P\left(y_n \in \mathcal{S}_j | \mathbf{s}_n[c_i]\right)$ in eq. (2.16).

Lemma 2 *Let $y_n = \mathbf{r}_p^T(\tau_e)\,\mathbf{s}_n + u_n$ as in (2.7) and let c_i, c_j be two points in $\mathcal{A}$ with regions $\mathcal{S}_i, \mathcal{S}_j$ as defined in Lemma 1, then*

$$P\left(y_n \in \mathcal{S}_j | \mathbf{s}_n[c_i]\right) = Q\left(\frac{\sqrt{2}\Re\left\{\left(y_n - \frac{c_i+c_j}{2}\right)(c_i - c_j)^*\right\}}{\sigma|c_i - c_j|}\right), \tag{2.17}$$

where

$$Q(x) = \int_x^\infty \frac{e^{-u^2/2}}{\sqrt{2\pi}} du. \tag{2.18}$$

Proof: See Appendix.

In eq. (2.17) $*$ represents complex conjugation and $\Re$ represents the real part. Substituting (2.17) in (2.16) and rearranging gives:

$$P(e) = \frac{1}{M} \sum_{i=1}^{M} E_{\mathbf{s}_n[c_i]} \sum_{j=1 j\neq i}^{M} Q\left(\frac{\sqrt{2}\Re\left\{\left(y_n - \frac{c_i+c_j}{2}\right)(c_i - c_j)^*\right\}}{\sigma|c_i - c_j|}\right). \tag{2.19}$$

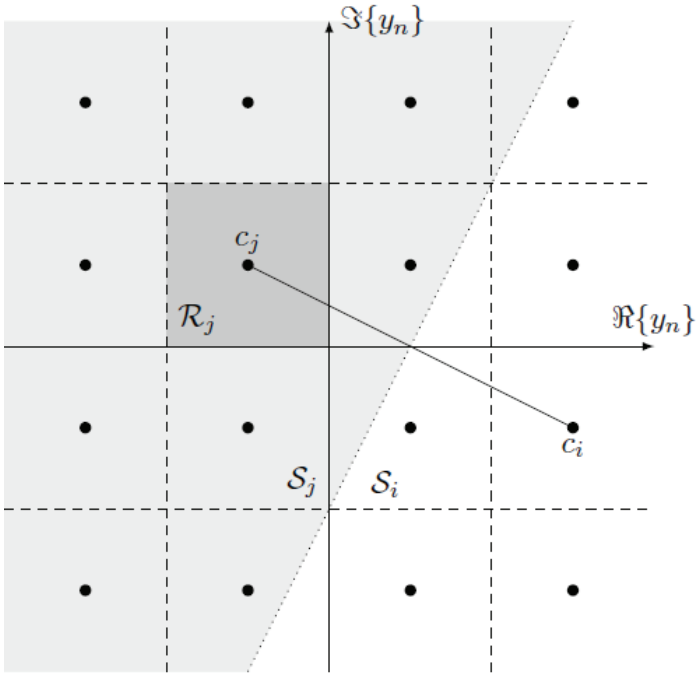

Fig. 2.1: 16-quadrature amplitude modulation (QAM) constellation.

Let

$$P_e(e) = \frac{1}{M}\sum_{i=1}^{M}\sum_{j=1 j\neq i}^{M} Q\left(\frac{\sqrt{2}\Re\left\{\left(y_n - \frac{c_i+c_j}{2}\right)(c_i-c_j)^*\right\}}{\sigma|c_i-c_j|}\right). \tag{2.20}$$

The derivative of $\log(P(e))$ with respect to τ_e using the principles from Brandwood [21] will lead to the error signal of the timing error detector,

$$e = \frac{d\log(P(e))}{d\tau_e} = \frac{1}{P_e(e)}\cdot\frac{dP(e)}{d\tau_e}, \tag{2.21}$$

where $\frac{dP(e)}{d\tau_e}$ is given by:

$$\begin{aligned}\frac{dP(e)}{d\tau_e} = \frac{1}{M}\sum_{i=1}^{M}\sum_{j=1 j\neq i}^{M} \exp\left(\frac{-1}{2\sigma^2}\left(\frac{\sqrt{2}}{|c_i-c_j|}\Re\left\{\left(y_n - \frac{c_i+c_j}{2}\right)(c_i-c_j)^*\right\}\right)^2\right) \\ \times\left(\frac{\sqrt{2}\Re\left\{\left(y_n - \frac{c_i+c_j}{2}\right)(c_i-c_j)^*\right\}}{\sigma|c_i-c_j|}\right).\end{aligned} \tag{2.22}$$

Here $\dot{y_n}$ is the derivative of y_n which is a function of τ_e.

Substituting (2.22) in (2.21) gives:

$$e = \frac{1}{P_e\left(e\right)} \cdot \frac{1}{M} \sum_{i=1}^{M} \sum_{j=1 j \neq i}^{M} \exp\left(\frac{-1}{2\sigma^2} \left(\frac{\sqrt{2}}{|c_i - c_j|} \Re\left\{ \left(y_n - \frac{c_i + c_j}{2} \right) \left(c_i - c_j\right)^* \right\} \right)^2 \right) \times \left(\frac{\sqrt{2} \Re\left\{ \left(\dot{y_n} - \frac{c_i + c_j}{2} \right) \left(c_i - c_j\right)^* \right\}}{\sigma |c_i - c_j|} \right). \tag{2.23}$$

Approximating the function $Q'(x)$ with $Q(x)$ (2.23) becomes:

$$e_a = \frac{1}{P_e\left(e\right)} \cdot \frac{1}{M} \sum_{i=1}^{M} \sum_{j=1 j \neq i}^{M} Q\left(\frac{1}{2\sigma^2} \left(\frac{\sqrt{2}}{|c_i - c_j|} \Re\left\{ \left(y_n - \frac{c_i + c_j}{2} \right) \left(c_i - c_j\right)^* \right\} \right)^2 \right) \times \left(\frac{\sqrt{2} \Re\left\{ \left(\dot{y_n} - \frac{c_i + c_j}{2} \right) \left(c_i - c_j\right)^* \right\}}{\sigma |c_i - c_j|} \right). \tag{2.24}$$

Equation (2.23) represents the exact timing error signal and (2.24) represents the approximate timing error. The symbols c_i, c_j, and y_n in (2.24) are complex numbers. Let $c_i = r1 + ir2$, $c_j = t1 + it2$ and $y_n = z1 + iz2$ where $r1, r2, t1, t2, z1, z2$ are real numbers and $i = \sqrt{-1}$. Substituting these in (2.23) and simplifying gives:

$$e_a = \frac{1}{P_e\left(e\right)} \cdot \frac{1}{M} \sum_{i=1}^{M} \sum_{j=1 j \neq i}^{M} Q\left(\frac{1}{2\sigma^2} \left(\frac{\sqrt{2}}{|c_i - c_j|} \Re\left\{ \left(y_n - \frac{c_i + c_j}{2} \right) \left(c_i - c_j\right)^* \right\} \right)^2 \right) \times \left(\frac{\sqrt{2}}{\sigma |c_i - c_j|} \left(\dot{z1} \left(r1 - t1\right) + \dot{z2} \left(r2 - t2\right) \right) \right). \tag{2.25}$$

This looks like the error signal for maximum likelihood case, but scaled by nonlinear terms.

2.3 S-Curves

The S-curve is a useful tool to gain an insight on the behavior of TEDs. The term $\dot{y_n}$ is a function of τ_e. It can be shown that if $\tau_e = 0$, then $e = 0$. However in order to analyze whether the implication works in the other direction, S-curves are used. The S-curves are obtained by plotting the error signal e or e_a with respect to τ_e and averaging the plot over

the symbols. For this purpose, define:

$$\bar{g}_{\mathrm{MSER}}(\tau_e) = E\{e\}, \tag{2.26}$$

where E represents the expectation with respect to the symbols. The function $\bar{g}_{\mathrm{MSER}}(\tau_e)$ measures the average value of error for a given timing offset τ_e . Using eqs. (2.23) and (2.24), the exact S-curves and approximate S-curves are obtained. Figures 2.2 - 2.5 show the S-curves for different signal-to-noise ratios. The curve in solid are the exact S-curves, the dashed ones are approximate S-curves, and for reference, MLTED S-curves are also plotted which are the dotted ones.

The interesting point to observe from the plots is that S-curves for MSERTED have higher slopes than MLTED S-curves. As the SNR increases, the slope of the exact S-curve for MSERTED increases at the origin whereas the approximate one flattens. Figures 2.6 - 2.9 show the normalized S-curves. The S-curves help in calculating the TED loop parameters. The slope of these curves at the origin gives the "gain" denoted K_p of the TED. The normalized S-curves provide the means for gain comparison of exact MSERTED, approximate MSERTED and the MLTED. The exact MSERTED and MLTED have pretty much the same gains at -10 dB. For 0 dB SNR the approximate MSERTED has higher gain than MLTED, whereas the exact MSERTED has pretty much the same behavior as MLTED. The S-curves from 5 dB onwards looks very interesting which shows us that the approximate MSERTED had higher gain than the ML case. At these SNRs the approximate MSERTED will amplify the timing errors as compared to MLTED and will lead to fast convergence. For SNRs greater than or equal to 10 dB, the step size in the adaptation process for approximate MSERTED is very high for high timing offset errors. The behavior of amplifying the error signal produces a large timing error and makes the approximate MSERTED adapt faster compared to MLTED. This is illustrated with the simulation results.

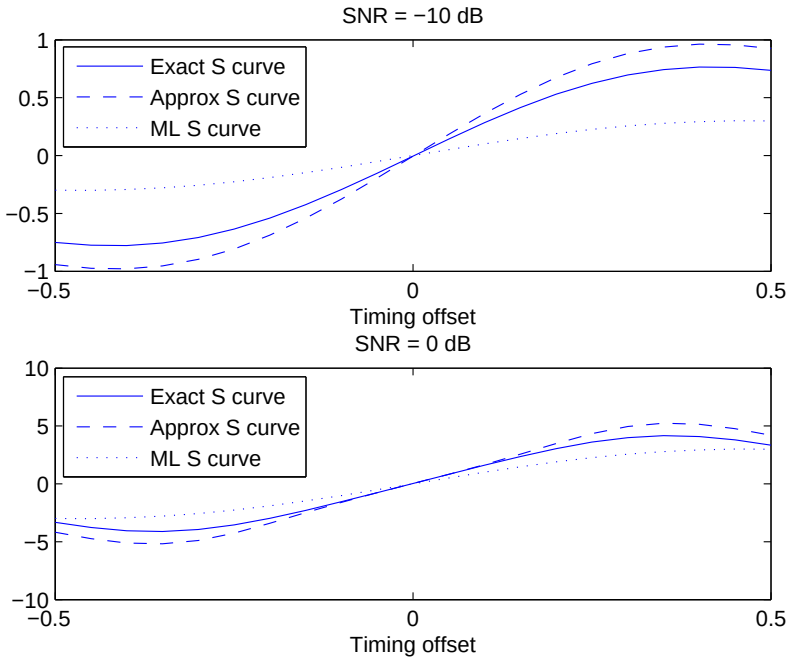

Fig. 2.2: S-curves at -10 dB and 0 dB.

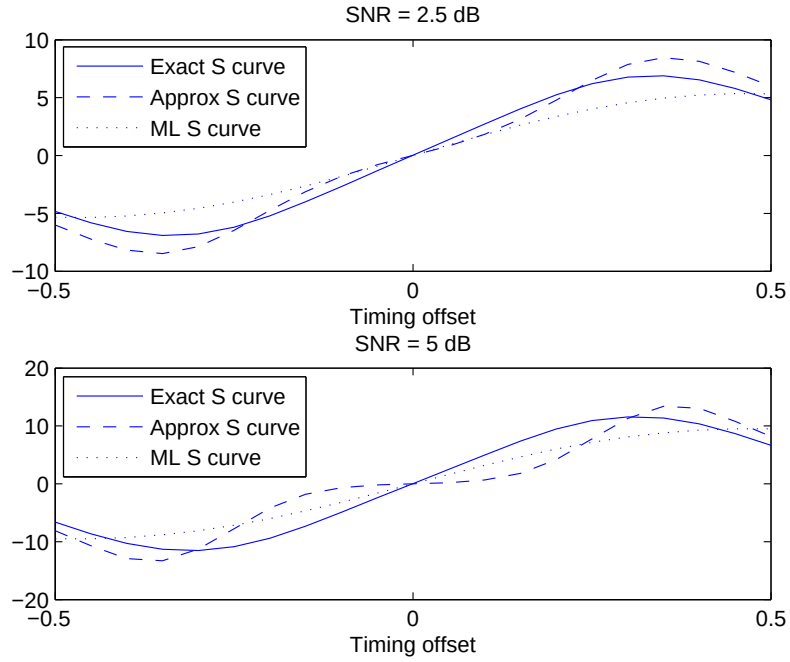

Fig. 2.3: S-curves at 2.5 dB and 5 dB.

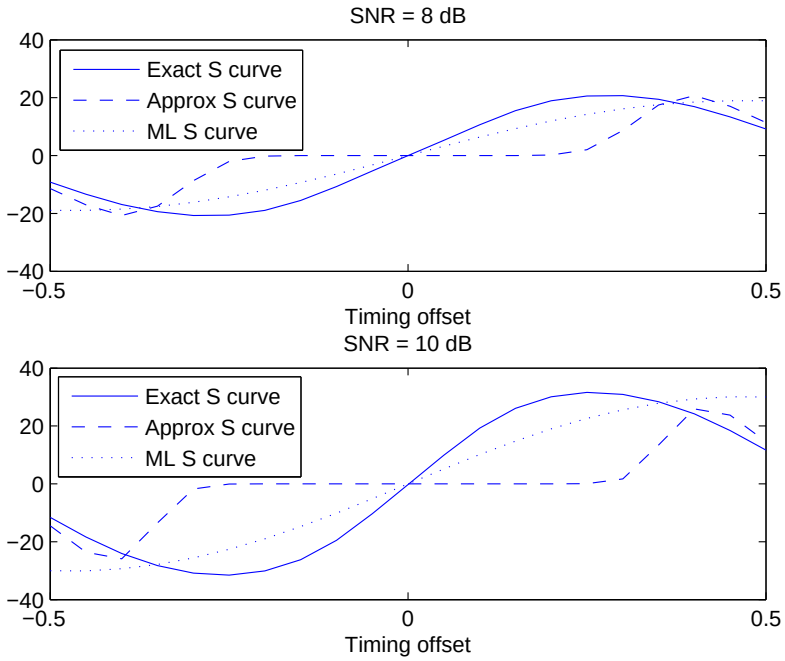

Fig. 2.4: S-curves at 8 dB and 10 dB.

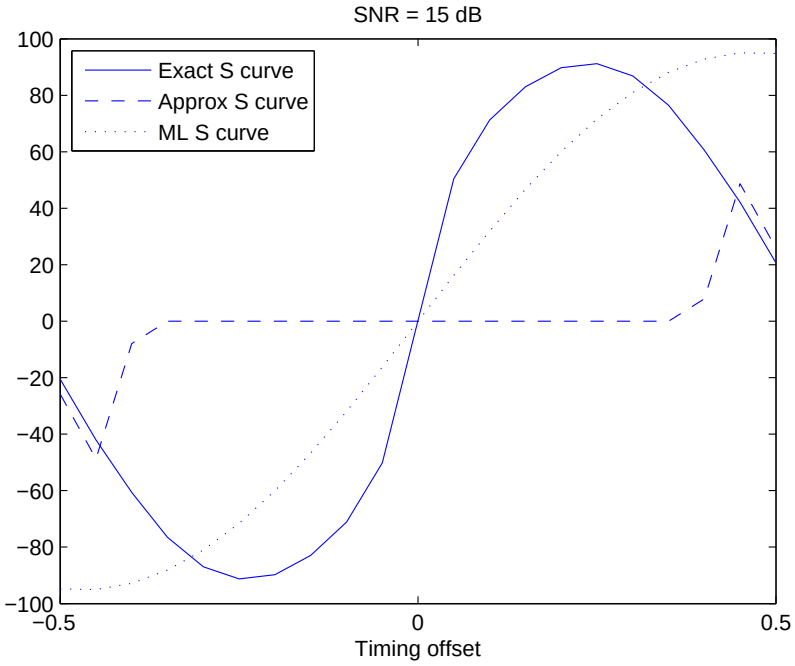

Fig. 2.5: S-curves at 15 dB.

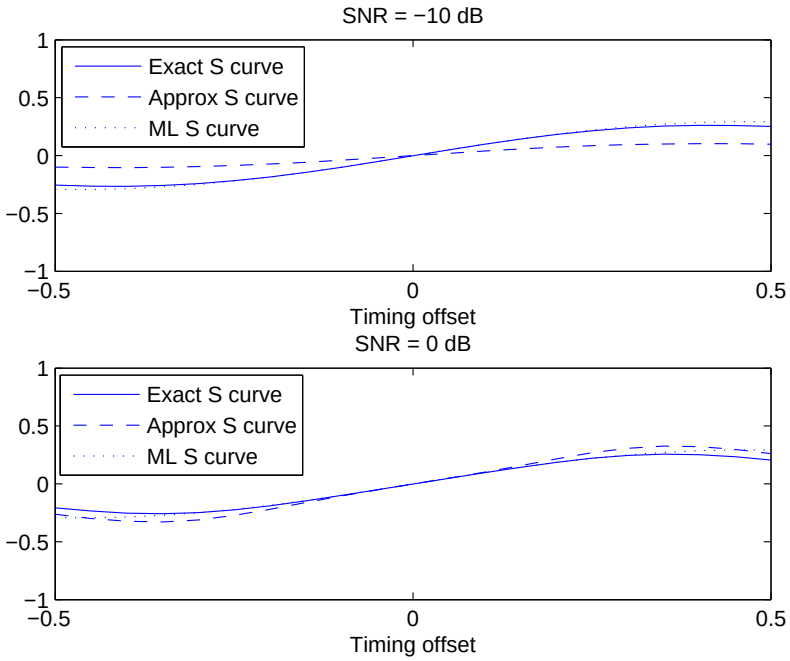

Fig. 2.6: Normalized S-curves at -10 dB and 0 dB.

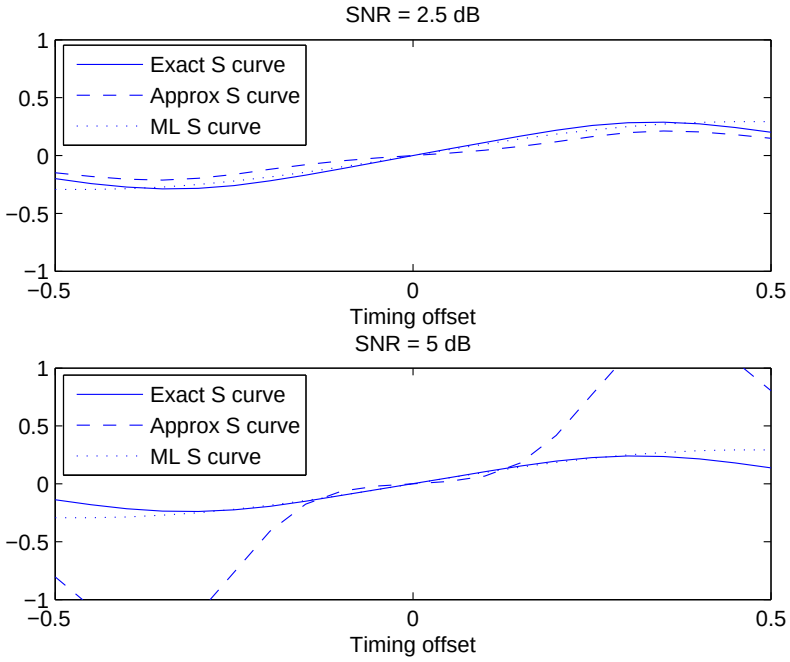

Fig. 2.7: Normalized S-curves at 2.5 dB and 5 dB.

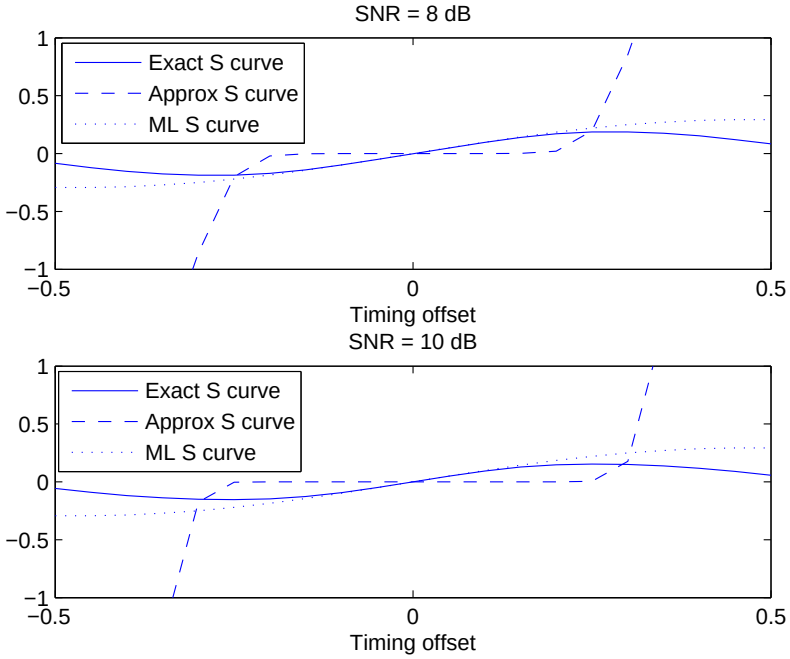

Fig. 2.8: Normalized S-curves at 8 dB and 10 dB.

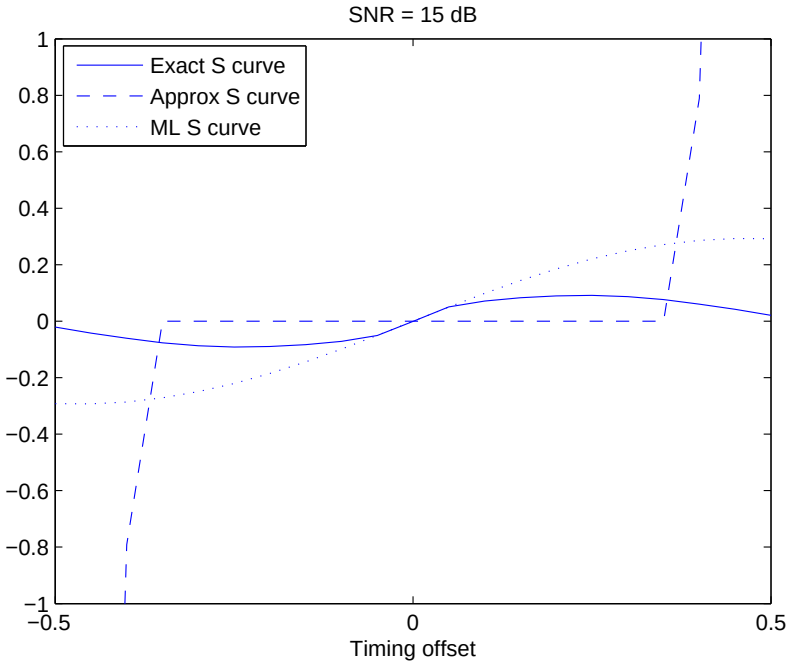

Fig. 2.9: Normalized S-curves at 15dB.

Chapter 3

Implementation

3.1 Transmitter Processing

This chapter describes the implementation details of the MSERTED. Figure 3.1 shows the processing at the transmitter section. Random bits are generated which are then mapped to symbols in the constellation space. The look up table (LUT) holds the symbols in the constellation. The symbols in the constellation have unit energy. The obtained symbol stream is then upsampled by a factor of N to avoid aliasing. Then the upsampled stream is then modulated by pulse shaping filter. The pulse used here is an SRRC pulse given by (3.1):

$$p\left(t\right)=\frac{1}{\sqrt{T_s}}\frac{\sin\left(\pi\left(1-\alpha\right)\frac{t}{T_s}\right)+\frac{4\alpha t}{T_s}\cos\left(\pi\left(1+\alpha\right)\frac{t}{T_s}\right)}{\frac{\pi t}{T_s}\left(1-\left(\frac{4\alpha t}{T_s}\right)^2\right)}, \tag{3.1}$$

where T_s is the sample period and α is the excess bandwidth. The SRRC used has a timing offset τ which needs to be estimated at the receiver. The signal then goes through a channel where additive white gaussian noise (AWGN) with variance σ^2 is added to the signal.

3.2 Receiver Processing

Figure 3.2 shows the receiver processing of the MSERTED. Note that $\dot{r}$, x, $\dot{x}$ are complex signals with in-phase in the real part and quadrature-phase in the imaginary part. In a practical situation the received data is sampled using an analog-to-digital converter (ADC). The sampled data $r(nT)$ is then processed using digital processing techniques. The receiver block consists of a matched filter with impulse response $p(-t)$, derivative matched filter, piecewise parabolic interpolator, error computation block, Butterworth filter, loop

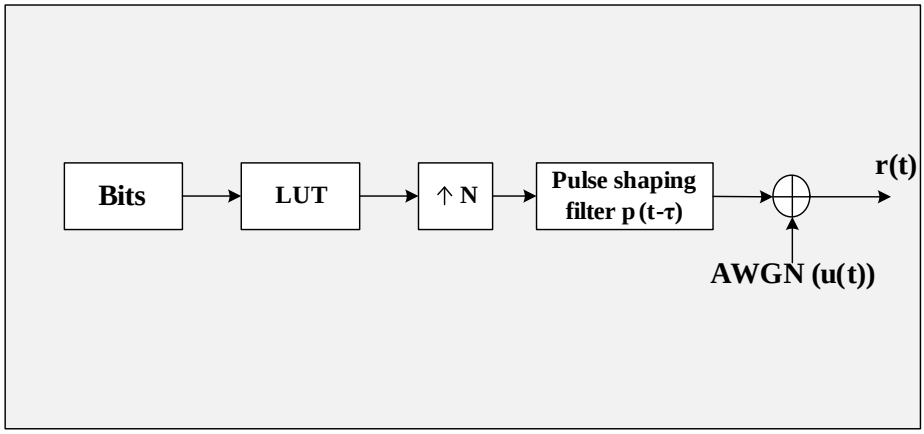

Fig. 3.1: Transmitter processing.

filter, numerically controlled oscillator (NCO), μ calculation block, and the decision block. The received samples are filter by MF and derivative MF, which operate in parallel on the received samples. The interpolator is used to obtain the intermediate samples using the available samples. The interpolation control block provides the interpolant given a base index and fractional interval μ which satisfies the condition $0 \leq \mu < 1$. The interpolator used here is a cubic interpolator with farrow structure [1] which is shown in fig. 3.3. There are two interpolators used. One computes the interpolants for the MF output, and the second one computes the outputs of the derivative MF. The modulo-1 counter-based interpolation control is used in the receiver. This scheme is used to accomplish the interpolation control where interpolants are required for every N samples. The modulo-1 counter used here is a decrementing counter. The counter is decremented in the steps of $1/N$, and hence on an average the counter underflows every N samples. Whenever there is an underflow signal, the μ value is updated. The underflow is used as control to generate the interpolants in the interpolator block. The outputs of the interpolator is given to a decision block which makes decisions based on the minimum distance criteria. The error computation block computes the error as per eq. (2.23) in case of exact MSERTED and as per eq. (2.24) in case approximate MSERTED. The error computation is done using the symbol decisions from the decision block, interpolator outputs operating on the MF and derivative MF outputs. The decrementing modulo-1 counter and the loop filter in this case operate at a higher

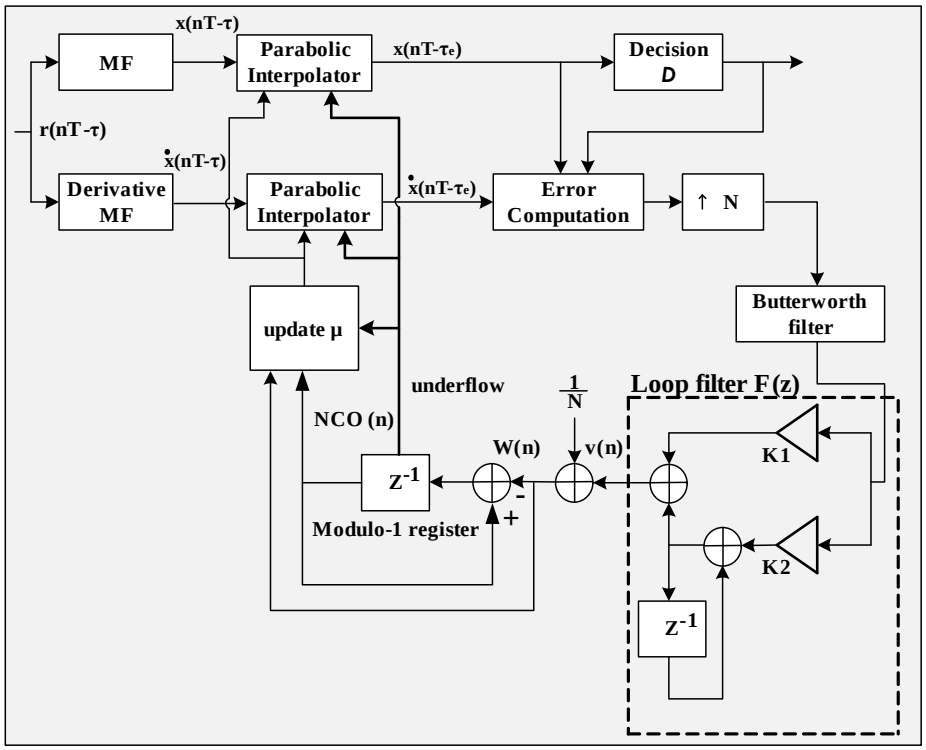

Fig. 3.2: Receiver processing.

rate of N samples per symbol period. Therefore, the error signal is upsampled by N. The upsampling is performed by inserting zeros between the updates of the error signal. The receiver block has a Butterworth filter which is used to smooth out the error signal. The output of the Butterworth filter then goes through the loop filter.

The loop dynamics of the loop filter are obtained using the K_p value from the S-curves. The calculation of loop parameters K_1 and K_2 are done using eqs. (3.2) and (3.3).

$$K1 = \frac{1}{K_p K_0} \frac{\frac{4\zeta}{N}\left(\frac{B_n T_s}{\zeta+\frac{1}{4\zeta}}\right)}{1+\frac{2\zeta}{N}\left(\frac{B_n T_s}{\zeta+\frac{1}{4\zeta}}\right)+\left(\frac{B_n T_s}{N\left(\zeta+\frac{1}{4\zeta}\right)}\right)^2} \tag{3.2}$$

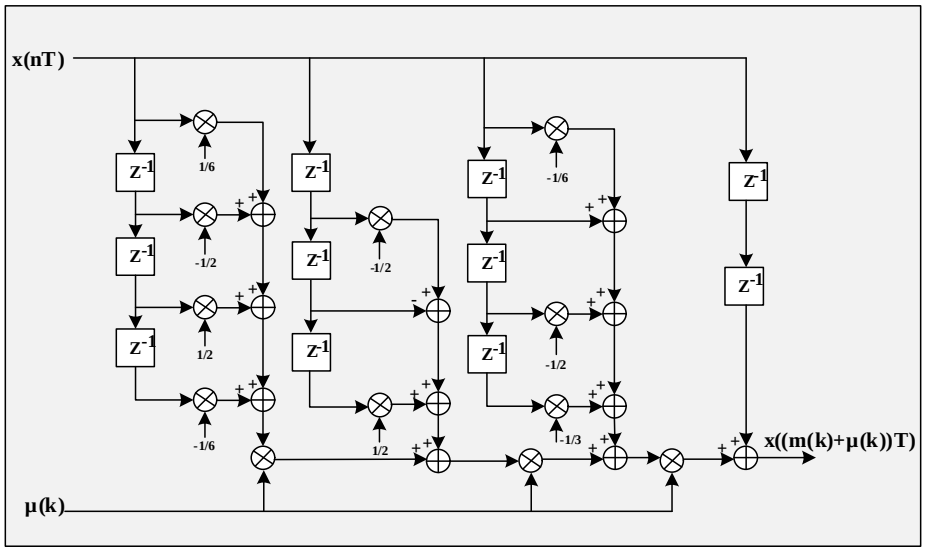

Fig. 3.3: Farrow Interpolator.

$$K1 = \frac{1}{K_p K_0} \frac{\frac{4\zeta}{N^2}\left(\frac{B_n T_s}{\zeta+\frac{1}{4\zeta}}\right)^2}{1+\frac{2\zeta}{N}\left(\frac{B_n T_s}{\zeta+\frac{1}{4\zeta}}\right)+\left(\frac{B_n T_s}{N\left(\zeta+\frac{1}{4\zeta}\right)}\right)^2}. \tag{3.3}$$

The term ζ is the damping factor of the loop filter. When $\zeta < 1$, the loop response exhibits damped oscillations and the system is called underdamped system. The poles are complex conjugate pairs. When $\zeta > 1$, the loop response is the sum of decaying exponentials and the system is called overdamped system. The poles of the system are real and distinct. When $\zeta = 1$, the system is called critically damped system. The loop response is between the damped oscillations and decaying exponentials. The poles are real and repeated. The term B_n is called noise bandwidth and is a linear function of ζ.

The complete system used for simulations consists of transmitter processing and receiver processing shown in figs. 3.1 and 3.2. This system is used to obtain the symbol error rate (SER) curves and error curves to substantiate the fast convergence and low symbol error rate of approximate MSERTED as compared to MLTED.

Chapter 4

Results

4.1 Probability of Error

This chapter discusses the results obtained by the simulation of MSERTED system. Equation (2.19) represents the probability of error as a function of τ for the MSERTED. Figure 4.1 shows the logarithm of probability of error as a function of τ for different SNR values. The simulations were done for QPSK constellation with unit energy symbols. For each value of τ the probability of error was averaged over 1000 trials of the experiment. The pulse shape used is SRRC pulse with 50% excess bandwidth and $L_p = 4$. The plots show that the probability of error is high for higher time offsets $\tau = 0.5Ts$ and $\tau = -0.5Ts$ and decreases as the timing offset decreases. The probability of error has minimum at $\tau = 0$. For SNRs greater than 10dB the probability of error decreases significantly.

4.2 Symbol Error Rate

The transmitter and receiver processing blocks shown in figs. 3.1 and 3.2, respectively, were used for the complete system simulations. The symbol error rate curves were obtained for approximate MSERTED and the MLTED for comparing the results. The S-curves also predicts that the exact MLTED might perform no better than MLTED. Hence, the comparison is done between the approximate MSERTED and MLTED. The approximate MSERTED is more practical as compared to the exact one since it has the Q function in its arguments rather than an exponential term.

The QPSK constellation is used for the simulation of the system. The received data was generated with timing offset $\tau = 0.5Ts$ with the noise added to it. In order to have a fair comparison the same loop dynamics for MSERTED and MLTED were used. The damping factor of $\zeta = 1/\sqrt{2}$ and (noise equivalent bandwidth)(symbol period) product of

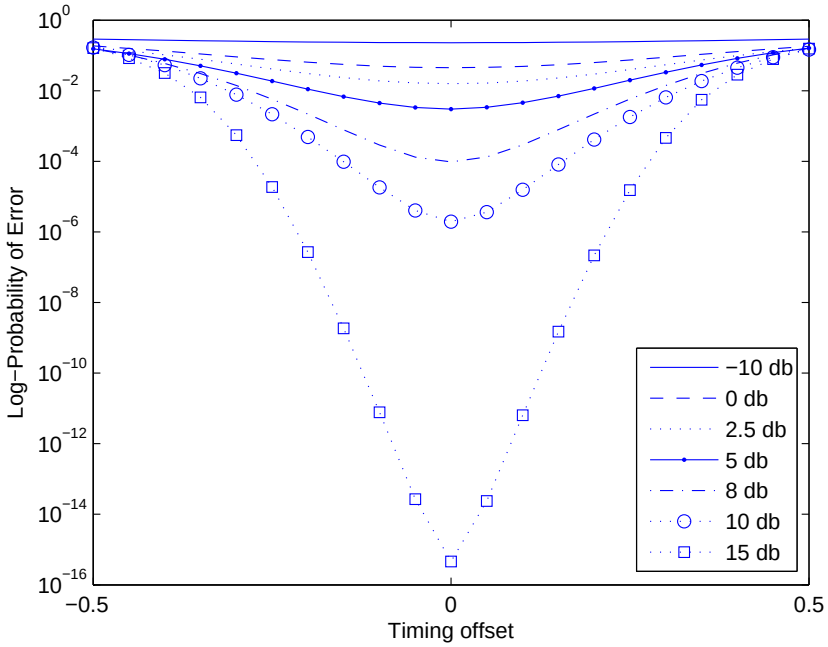

Fig. 4.1: Log-probability of error at various SNRs.

$B_nT_s = 0.005$ were used. The parameter that changes for the two TEDs is the K_p which in turn gives K_1 and K_2. As the TEDs adapted, the symbol errors were counted each time for 1000 symbols and were averaged over 5,000 trials of the experiment. The obtained symbol error probability is plotted over time. Figures 4.2 - 4.5 show the symbol error rate curves for different SNR values. The curve in blue is for MLTED and the curve in red is for approximate MSERTED. The symbol error rate (SER) curve at -10 dB shows that the approximate MSERTED and MLTED converge at the same time but the MSERTED has a lower steady state error than MLTED. At 0 dB and 2.5 dB, ML and MSER have nearly the same performance both in convergence and steady state symbol error rate. The MSERTED performs extremely well for all other SNRs. As shown in fig. 4.3, at 5 dB, MSERTED converges faster than ML and also has the lower steady state error. At SNRs 10 dB and 15 dB, the MSERTED converges faster than ML and also has lower steady state error compared to ML. This is illustrated in figs. 4.4 and 4.5. One can see that MSER has improved damping near the convergence point. This can be seen in the adaptation curves. The MLTED undergoes an oscillatory mode before converging to a solution whereas

MSERTED oscillations decays rapidly.

The same system was simulated with a timing offset $\tau = 0.25Ts$ for the SNRs 8 dB and 10 dB. Figure 4.6 shows the symbol error rate plots. It can be seen that the MSERTED converges faster and have either low steady error or no errors compared to MLTED.

4.3 Error Signal Plots

The error signal is the output of the timing detector, which gives the information about the convergence of the system towards a solution. Figures 4.7 - 4.10 show the error signals of the approximate MSERTED and MLTED. The curve in blue is for MLTED, and the curve in red is for approximate MSERTED. At -10 dB one can observe that both MSER and ML converge at the same time, but the error signal amplitude is less for MSER compared to ML, and hence low steady state error. At 0 dB and 2.5 dB, both MSER and ML curves look similar, and from 5 dB onwards one can observe the faster convergence and low error amplitude at the steady state. We can also observe that the MSERTED has improved damping performance compared to MLTED. The MLTED oscillates more before reaching the convergence point where as MSERTED has fast decaying oscillations near the convergence point. These signals exactly correspond to the behavior exhibited by the SER curves.

At the optimum sampling instant, the timing error is zero when there is data transition. When there is no data transition, even at the optimum sampling instant, the timing error may not be zero. This nonzero value is called self noise of the TED. Figure 4.11 shows a typical plot of μ. The simulation was done for a timing offset of $\tau = 0.4Ts$ at 8 dB SNR. We can observe that μ in case of MSERTED tries to settle faster than MLTED, but μ for ML is more smoother than MSERTED and takes more time to settle at 0.6. This shows that MSERTED has higher self noise than MLTED. This high self noise is due to the high gain to the MSERTED.

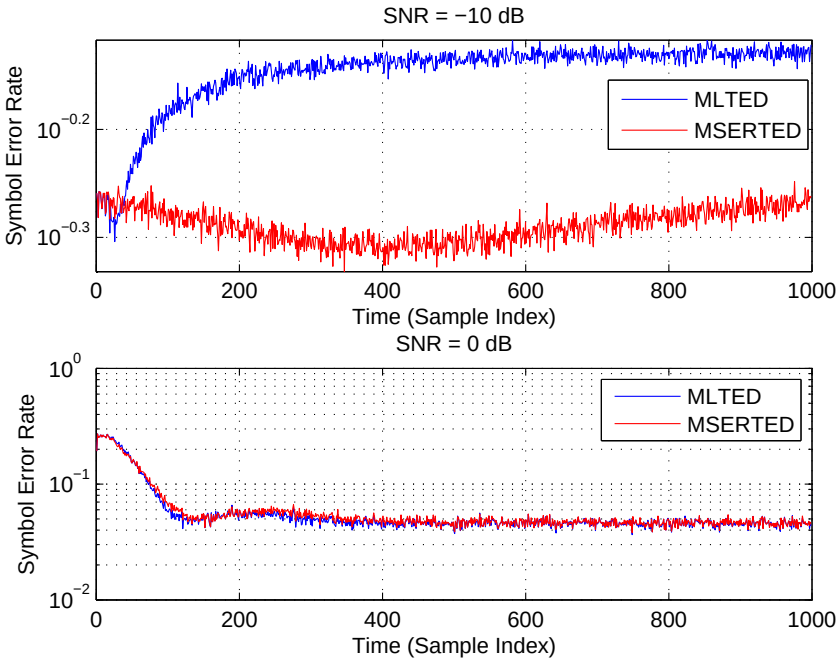

Fig. 4.2: Symbol error rates at -10 dB and 0 dB.

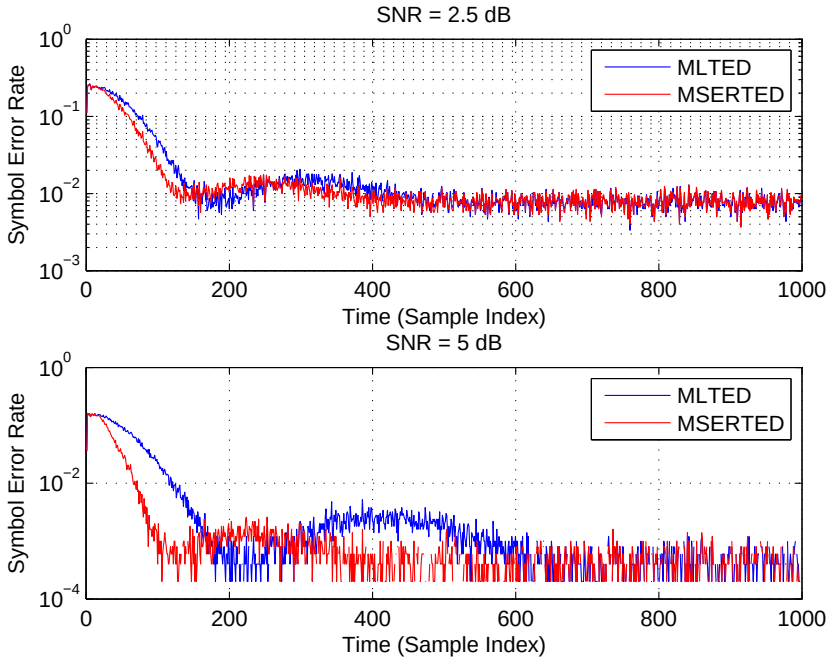

Fig. 4.3: Symbol error rates at 2.5 dB and 5 dB.

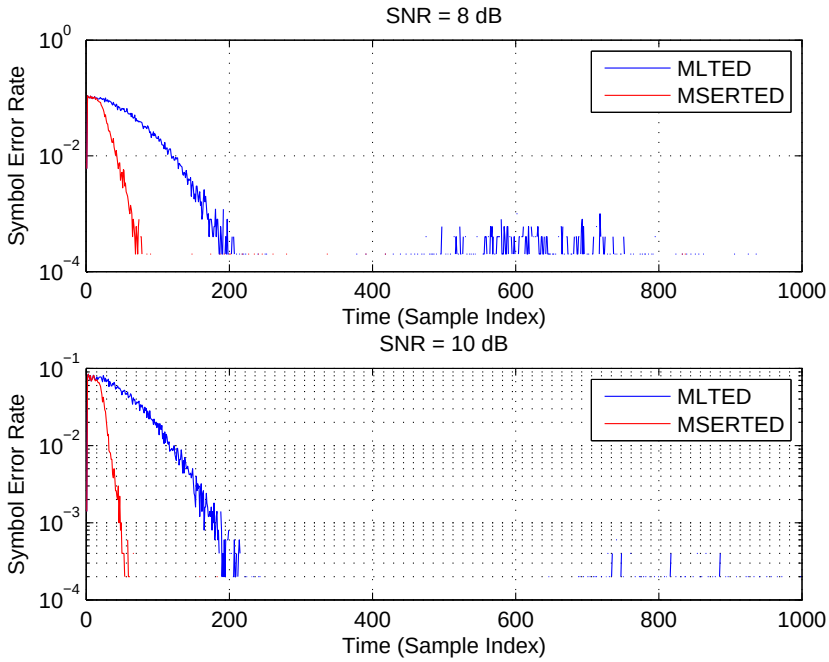

Fig. 4.4: Symbol error rates at 8 dB and 10 dB.

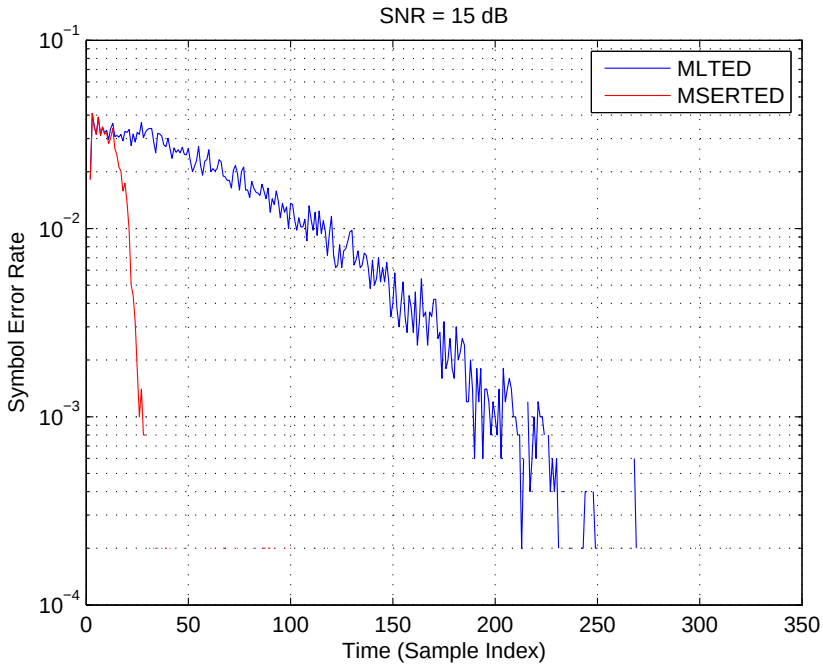

Fig. 4.5: Symbol error rate at 15 dB.

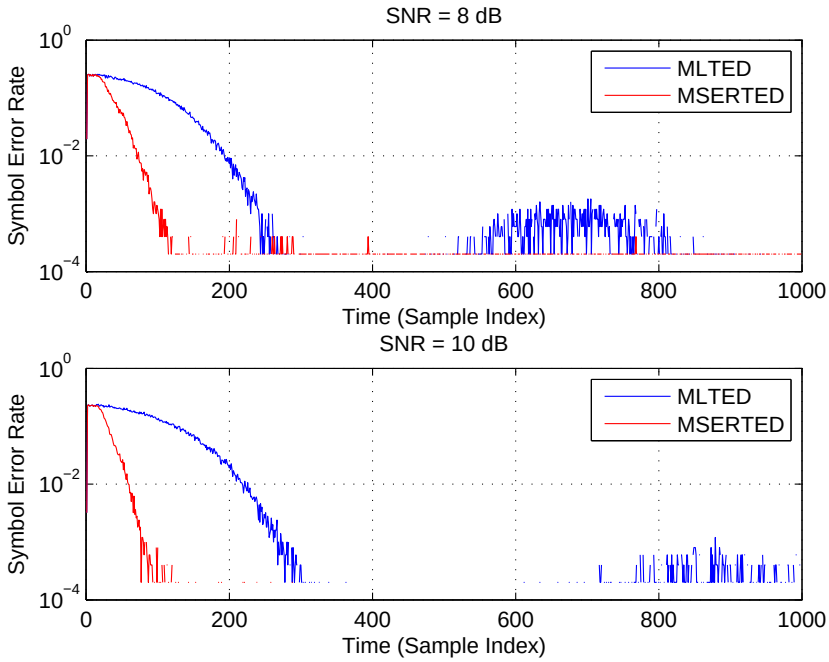

Fig. 4.6: Symbol error rates at 8 dB and 10 dB for $\tau = 0.25Ts$.

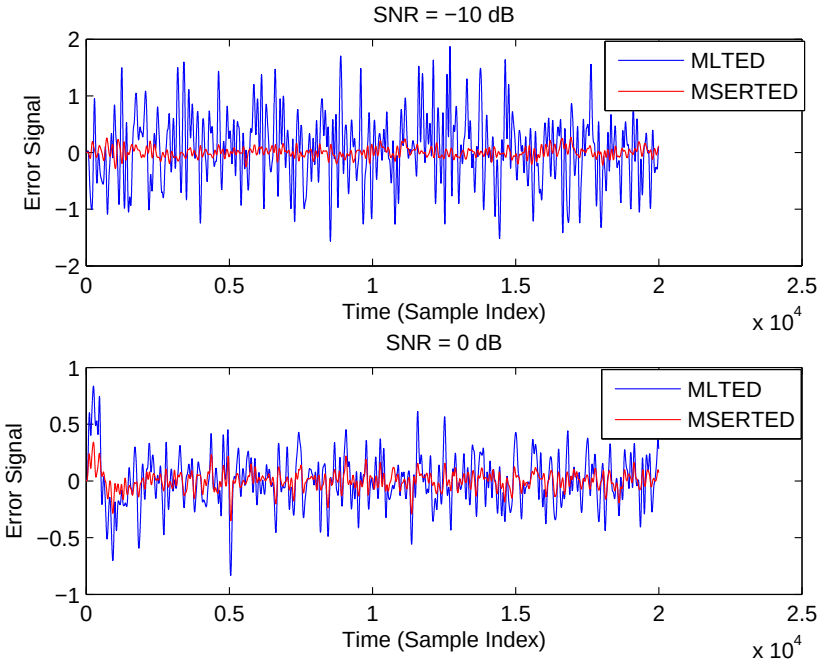

Fig. 4.7: Error signals at -10 dB and 0 dB.

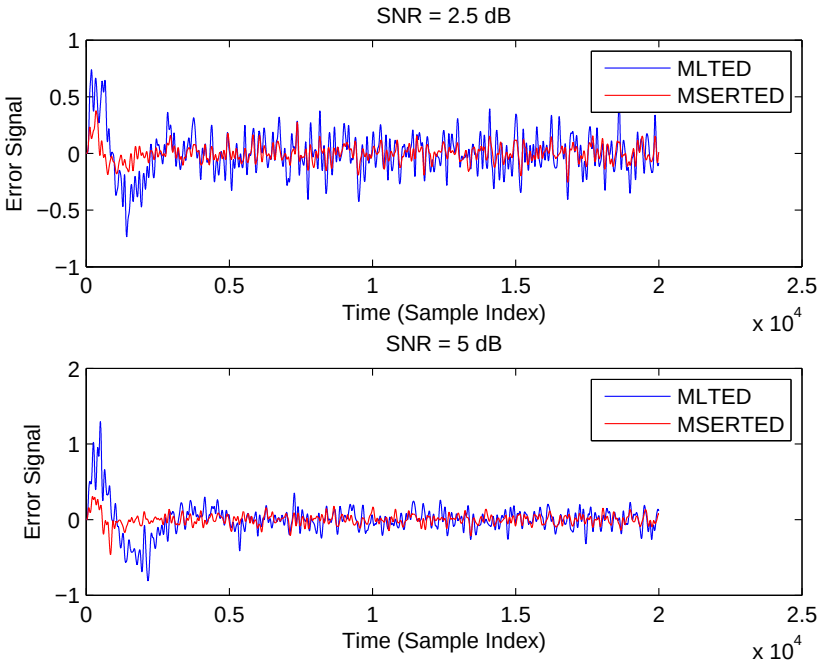

Fig. 4.8: Error signals at 2.5 dB and 5 dB.

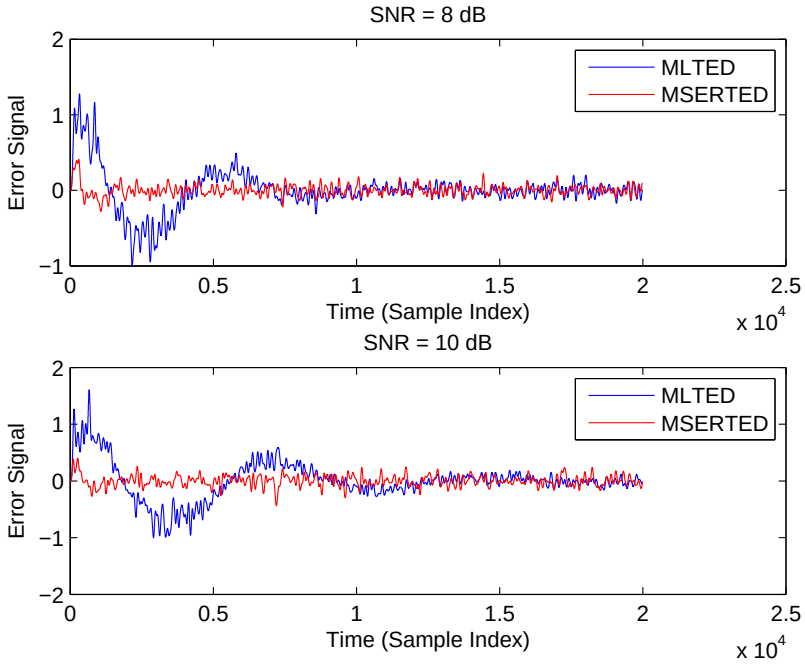

Fig. 4.9: Error signals at 8 dB and 10 dB.

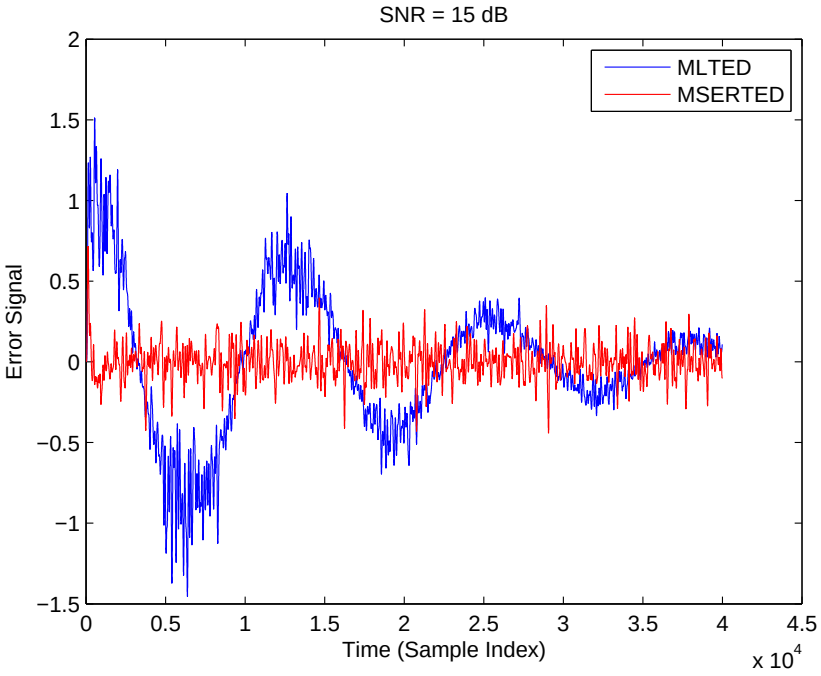

Fig. 4.10: Error signal at 15 dB.

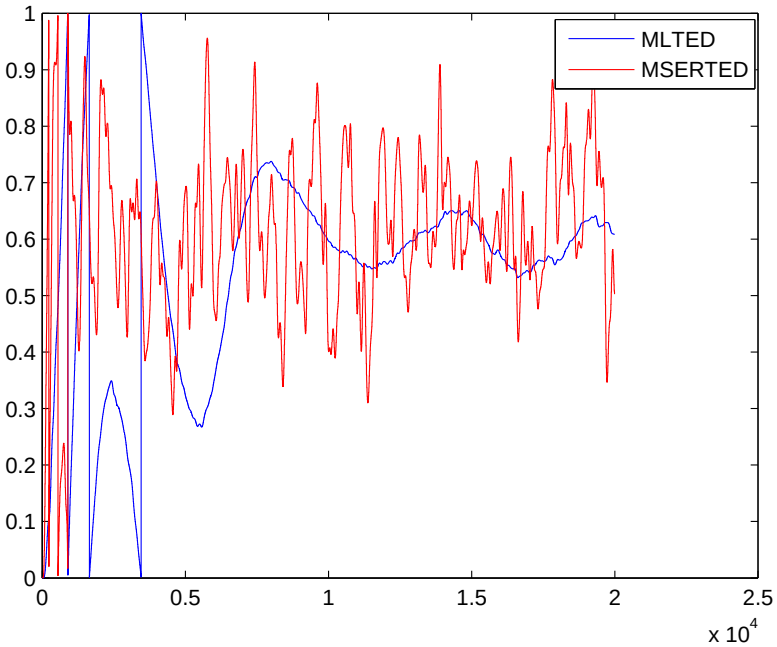

Fig. 4.11: An example μ plot.

4.4 Clock Frequency Offset

This section deals with the problem of clock frequency offset. The clock frequency offset makes the constellation continuously rotate and scatter the symbols over the entire constellation. The new TED proposed also works better than ML in compensating the clock frequency offset. The same system is used for the simulation with the same loop dynamics. The error signals are plotted for frequency offsets of 0.0025 and 0.005 for SNRs 5 dB and 8 dB, respectively. The plots are shown in fig. 4.12. We can observe that MSERTED converges faster than MLTED, and hence MSERTED has a better performance than MLTED in case of clock frequency offset as well.

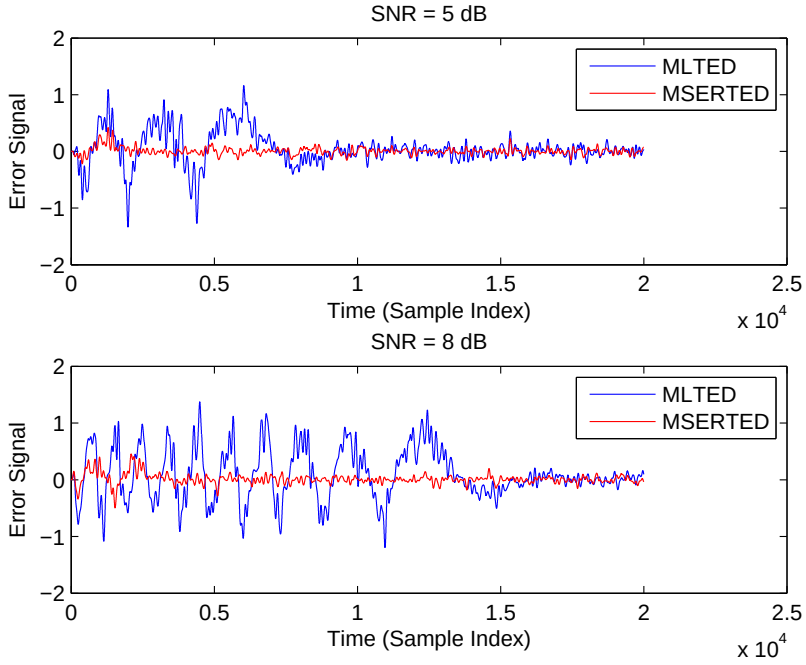

Fig. 4.12: Error signals for frequency offset of 0.0025 at 5 dB and 8 dB.

Chapter 5

Conclusion and Future Work

5.1 Conclusion

This thesis discusses the development and testing a new timing error detector which minimizes the symbol error probability. The development holds good for any constellation though the results presented are for QPSK constellation. The expressions for two timing error detectors namely exact MSERTED and approximate MSERTED were derived. The approximate MSERTED performs better than the traditional MLTED. The new TEDs look like MLTED with nonlinear multiplicative terms. The other advantage of using the approximate expression is the practical feasibility of the implementation. Since the expression has a Q function it can fit into designs with a Q function look-up table. The S-curves were used as a tool to gain an insight of the behavior of the TEDs. The sumbol error rate, the error signal output of the TEDs, show that the approximate MSERTED converge and reach steady state faster than MLTED. The plots also show that MSERTED have lower symbol error rate than MLTED. Another conclusion is that we can have shorter training sequences in case of MSERTED to achieve timing synchronization than MLTED.

5.2 Future Work

The new TED developed has a complex algorithm as compared to MLTED. In order to achieve faster convergence and minimum symbol error rate the cost paid is the complex calculations involved with the new TED. Hence in future work, it will be good if the complexity of the algorithm is reduced so that it is quite easy to implement. However, the approximate MSERTED can be implemented using a look up table for Q function and interpolation techniques.

The new TED developed can be integrated with the minimum symbol error rate phase

recovery system developed by Gunther and Moon [5] as a future work. The new joint phase and timing recovery system can be designed and tested against ML case for the symbol error rate performance.

In future work, it might be a good idea to apply error correction coding techniques [22] in conjunction with the new TED presented to achieve better performance and more reliable communication.

References

[1] M. Rice, *Digital Communications: A Discrete-Time Approach*. Upper Saddle River, NJ: Pearson Prentice Hall, 2009.

[2] J. G. Proakis, *Digital Communications*. New York: McGraw-Hill, 2008.

[3] L. Franks, "Carrier and bit synchronization in data communication–A tutorial review," *IEEE Transactions on Communications*, vol. 28, no. 8, pp. 1107–1121, Aug. 1980.

[4] M. Meyers and L. Franks, "Joint carrier phase and symbol timing recovery for PAM systems," *IEEE Transactions on Communications*, vol. 28, no. 8, pp. 1121–1129, Aug. 1980.

[5] J. Gunther and T. Moon, "Minimum Symbol Error Rate Carrier Phase Recovery of QPSK," *IEEE Transactions on Signal Processing*, vol. 57, no. 8, pp. 3101–3107, Aug. 2009.

[6] M. Aaron and D. Tufts, "Intersymbol interference and error probability," *IEEE Transactions on Information Theory*, vol. 12, no. 1, pp. 26–34, Jan. 1966.

[7] R. Yen, "Stochastic Unbiased Minimum Mean Error Rate Algorithm for Decision Feedback Equalizers," *IEEE Transactions on Signal Processing*, vol. 55, no. 10, pp. 4758–4766, Oct. 2007.

[8] S. Chen, L. Hanzo, and B. Mulgrew, "Adaptive minimum symbol-error-rate decision feedback equalization for multilevel pulse-amplitude modulation," *IEEE Transactions on Signal Processing*, vol. 52, no. 7, pp. 2092–2101, July 2004.

[9] J. Gunther and T. Moon, "Minimum Bayes Risk Adaptive Linear Equalizers," *IEEE Transactions on Signal Processing*, vol. 57, no. 12, pp. 4788–4799, Dec. 2009.

[10] C.-C. Yeh and J. Barry, "Adaptive minimum bit-error rate equalization for binary signaling," *IEEE Transactions on Communications*, vol. 48, no. 7, pp. 1226–1235, July 2000.

[11] C.-C. Yeh and J. Barry, "Adaptive minimum symbol-error rate equalization for quadrature-amplitude modulation," *IEEE Transactions on Signal Processing*, vol. 51, no. 12, pp. 3263–3269, Dec. 2003.

[12] C.-C. Yeh, R. Lopes, and J. Barry, "Approximate minimum bit-error rate multiuser detection," in *Global Telecommunications Conference, 1998. The Bridge to Global Integration, GLOBECOM 98. IEEE*, vol. 6, pp. 3590–3595, 1998.

[13] S. Chen, A. Samingan, B. Mulgrew, and L. Hanzo, "Adaptive minimum-BER linear multiuser detection for DS-CDMA signals in multipath channels," *IEEE Transactions on Signal Processing*, vol. 49, no. 6, pp. 1240–1247, June 2001.

[14] X. Wang, W.-S. Lu, and A. Antomiou, "Constrained minimum-BER multiuser detection," *IEEE Transactions on Signal Processing*, vol. 48, no. 10, pp. 2903–2909, Oct. 2000.

[15] I. Psaromiligkos, S. Batalama, and D. Pados, "On adaptive minimum probability of error linear filter receivers for DS-CDMA channels," *IEEE Transactions on Communications*, vol. 47, no. 7, pp. 1092–1102, July 1999.

[16] S. Chen, L. Hanzo, and N. Ahmad, "Adaptive minimum bit error rate beamforming assisted receiver for wireless communications," in *IEEE International Conference on Acoustics, Speech, and Signal Processing (ICASSP)*, vol. 4, pp. IV–640, 2003.

[17] T. Samir, S. Elnoubi, and A. Elnashar, "Class of minimum bit error rate algorithms," in *The 9th International Conference on Advanced Communication Technology*, vol. 1, pp. 168–173, 2007.

[18] J. Bergmans and H. Wong-Lam, "A class of data-aided timing-recovery schemes," *IEEE Transactions on Communications*, vol. 43, no. 234, pp. 1819–1827, Feb./Mar./Apr. 1995.

[19] F. Gardner, "A BPSK/QPSK timing-error detector for sampled receivers," *IEEE Transactions on Communications*, vol. 34, no. 5, pp. 423–429, May 1986.

[20] K. Mueller and M. Muller, "Timing recovery in digital synchronous data receivers," *IEEE Transactions on Communications*, vol. 24, no. 5, pp. 516–531, May 1976.

[21] D. Brandwood, "A complex gradient operator and its application in adaptive array theory," *IEE Proceedings on Microwaves, Optics and Antennas*, vol. 130, no. 1, pp. 11–16, Feb. 1983.

[22] T. Moon, *Error Correction Coding: Mathematical Methods and Algorithms*. Hoboken, NJ: Wiley Interscience, 2006.

Appendix

Q-function Proof

In this appendix we examine the probability on the right hand side of (2.15) which is the probability that the matched filter output is closer to c_j than to the transmitted symbol c_i. The principles in this proof are used from the paper by Gunther and Moon [9]. First, note that the event:

$$\left\{|y_n - c_j|^2 < |y_n - c_i|^2 \middle| \mathbf{s}_n[c_i]\right\},$$

is equivalent to the event:

$$\left\{0 < \Re\left\{\left(y_n - \frac{c_j + c_i}{2}\right)(c_j - c_i)^*\right\} \middle| \mathbf{s}_n[c_i]\right\}. \tag{7.1}$$

Next, substitute the model (2.7) into (7.1) to obtain:

$$\left\{0 < \Re\left\{\left(u_n + \mathbf{r}_p^T(\tau_e)\,\mathbf{s}_n - \frac{c_j + c_i}{2}\right)(c_j - c_i)^*\right\} \middle| \mathbf{s}_n[c_i]\right\}. \tag{7.2}$$

The rearranging of (7.2) yields:

$$\left\{\Re\left\{-u(c_i - c_j)^*\right\} > \Re\left\{\left(\mathbf{r}_p^T(\tau_e)\,\mathbf{s}_n - \frac{c_i + c_j}{2}\right)(c_i - c_j)^*\right\} \middle| \mathbf{s}_n[c_i]\right\}. \tag{7.3}$$

Note that $-u$ can be replaced by u because they have the same distribution. Now, if u is zero mean and Gaussian with variance σ^2, then $v = u(c_i - c_j)^*$ is Gaussian with variance of $|c_i - c_j|^2\sigma^2$ and the real part of $v = v_r + jv_i$ has variance ${\sigma_r}^2 = |c_i - c_j|^2\sigma^2/2$. The probability of the even in (7.3) is computed as follows:

$$\begin{aligned} P(v_r > z|\mathbf{s}_n[c_i]) &= \int_z^\infty \frac{e^{-v_r^2/2\sigma_r^2}}{\sqrt{2\pi\sigma_r^2}}, \quad \nu = v_r/\sigma_r \\ &= \int_{z/\sigma_r^2}^\infty \frac{e^{-\nu^2/2}}{\sqrt{2\pi}} d\nu \\ &= Q(z/\sigma_r). \end{aligned} \tag{7.4}$$

Substituting the definitions of z and σ_r yields:

$$Q\left(\frac{\sqrt{2}\Re\left\{\left(\mathbf{r}_p^T\left(\tau_e\right)\mathbf{s}_n - \frac{c_i+c_j}{2}\right)\left(c_i-c_j\right)^*\right\}}{\sigma|c_i-c_j|}\right). \tag{7.5}$$

Substituting the model from (2.7) into (7.5) gives:

$$Q\left(\frac{\sqrt{2}\Re\left\{\left(y_n - \frac{c_i+c_j}{2}\right)\left(c_i-c_j\right)^*\right\}}{\sigma|c_i-c_j|}\right). \tag{7.6}$$